Abyssal Pathways and the Double Silica Maximum in the Northeast Pacific Basin

Susan L. Hautala[1] and Douglas E. Hammond[2]

[1]University of Washington.

[2]University of Southern California.

Corresponding author: Susan Hautala (hautala@uw.edu)

Key Points:

- An upper (North Pacific Deep Water) silica maximum is advecting through this region with only minor modification
- A lower (Upper Circumpolar Deep Water) maximum is created locally by lateral flow pathways and enhanced subarctic seafloor flux
- The existence of the double silica maximum is linked to weak diapycnal mixing, with broader implications for North Pacific overturning

Abstract

Causes of the double silica maximum in the deep Northeast Pacific Basin (NEPB) are explored using a stochastic Lagrangian approach. Steady-state advective fields, and diapycnal diffusion, are taken from a basin-scale hydrographic inverse method that conserves potential vorticity and salinity. Lateral diffusion is adjusted to optimize the overall agreement with radiocarbon. It is found that while the mid-depth silica maximum is not created locally, the near-bottom maximum is created within the eastern subarctic NEPB, by the combination of equatorward abyssal flow pathways and a latitude-dependent seafloor source. The existence of the double silica maximum requires weak diapycnal transport in the deep and bottom water, with implications for the conceptual picture of meridional overturning circulation in the North Pacific as a whole.

Plain Language Summary

Silica, an important nutrient supporting diatom production, has two distinct vertical concentration maxima in the deep (>1000 m) northeast Pacific ocean. This structure suggests that distinct processes create each of these features, but those processes have eluded explanation. Here, we explore how large-scale deep ocean currents from a recent study combine with a simple latitude-dependent source of silica from seafloor sediments to create the near-bottom maximum, a process that is confined to a southward current in the densest layers in the eastern half of the basin. In contrast, the shallower (mid-depth) silica maximum is already present in the inflowing deep water, and is not substantially modified as it flows through this part of the ocean.

1 Introduction

Deep water mass modification in the Northeast Pacific Basin (NEPB) is one of its least understood processes. Indicators of water "age", such as radiocarbon, are intensified at mid-depth, and the region has been described as a *cul-de-sac* of the planetary overturning circulation, where abyssal water is converted into mid-depth water by unresolved processes (e.g. Schmitz 1995). The existence of a double maximum in silica concentation (Si) – one near 2500 m, and another at the bottom near 4000 m (Edmond et al., 1979) – contraindicates direct upwelling of bottom water and raises questions about how these two maxima are maintained (Talley and Joyce 1992). Understanding the double Si maximum involves discarding oversimplified notions about one-dimensional advection/diffusion balances. In this study, three-dimensional, steady-state advection fields from a recent hydrographic inverse model (Hautala 2018) are used in a stochastic Lagrangian forward simulation of silica, carbon and radiocarbon concentration. Because the Mendocino Fracture Zone presents a barrier to meridional flow across ~40°N except in the westernmost NEPB, distinct pools of dense Lower Circumpolar Deep Water fill deep isolated areas to the north and south of this barrier. The analysis is thus confined to the North Pacific Deep Water (NPDW, $28.01 > \gamma > 27.70$) and Upper Circumpolar Deep Water ($28.10 > \gamma > 28.01$) following the definitions of MacDonald et al. (2009).

2 Methods

2.1 Boundary conditions

Lagrangian trajectories are initialized near the boundaries of the inverse model domain. Initial concentration values on selected neutral surfaces were defined with Ocean Data View using the GLODAPP data base to select and then interpolate existing tracer profiles (see Supplement, Figure S-A1). A northern initialization line (Figure 1c) roughly parallels the Aleutian Trench from (51°N, 180°) to (56.7°N, 137°N) at ~4° longitude spacing. Western and southern lines are defined at 180° (P14 section) and at 21°N (interpolating values from the P3 and P4 sections). A short southeastern line from 20°N to 30°N along 121°W also linearly interpolates the P3 and P4 sections.

2.2 Lagrangian trajectories

100 ensembles are initialized, each seeding 162 Lagrangian trajectories on each of 24 neutral surfaces within the UCDW and NPDW neutral density range (28.099 > γ > 27.615). The spacing is nominally 1°, linearly interpolating initial concentrations described above. If the meridional component of velocity at a seed location along the northern line is northward (out of the domain), then the location on that neutral surface is not initialized. If a seed location occurs north of the inverse model domain, the point is shifted along longitude lines to the northernmost inverse location, as long as it remains north of 47°N. We thereby make an assumption that, where the deepest neutral surfaces ground at varying longitudes on shoaling topography, a strictly southward flow supplies tracer from the Aleutian deep boundary current system (Warren and Owens 1985) to the closest point in the inverse domain. Such an assumption is consistent with interior abyssal circulation in this region (Hautala 2018), although there may be minor modification of tracer concentration along these short sections. Because the inverse model is designed to resolve the weaker large-scale interior circulation (based on a planetary geostrophic formulation for potential vorticity conservation), it does not resolve narrow, swift currents, such as the Aleutian deep boundary current system.

Using a 6-month time step, Δt, water parcel locations along Lagrangian trajectories are iterated from their previous location using a two stage calculation as follows. In a first (advective) stage, a displacement vector, $\underline{\Delta x} = (u\Delta t, v\Delta t, \Delta\eta + e\Delta t)$, is calculated using eastward (u) and northward (v) geostrophic velocity components, and the diapycnal velocity (e), from the hydrographic inverse model. The isoneutral component of vertical displacement, $\Delta\eta$, is the difference between the neutral surface height at the new position and the previous time step. Values between inverse model grid points are determined by linear interpolation. In a second (diffusive) stage, water parcels are randomly displaced by a value drawn from a Gaussian distribution with a specified standard deviation as follows.

Diapycnal stochastic displacements are based on diapycnal diffusivity, K_V, produced by the inverse model. Each inverse model geographical location yields a unique coefficient multiplying a vertical structure function motivated by observations (Kunze et al. 2006) and depending on stratification, bottom roughness and height above the bottom (see Hautala 2018 for details). The diapycnal displacement standard deviation, $\sqrt{2K_V\Delta t}$ (e.g., Taylor 1921), is thus a three-dimensional field. Diapycnal mixing has weak interior values and isolated mixing hotspots. The maximum isoneutral average is only 2.4×10^{-6} m^2 s^{-1} (corresponding to σ = 6 m after 6 months) found on a neutral surface with a mean depth of ~4200 m.

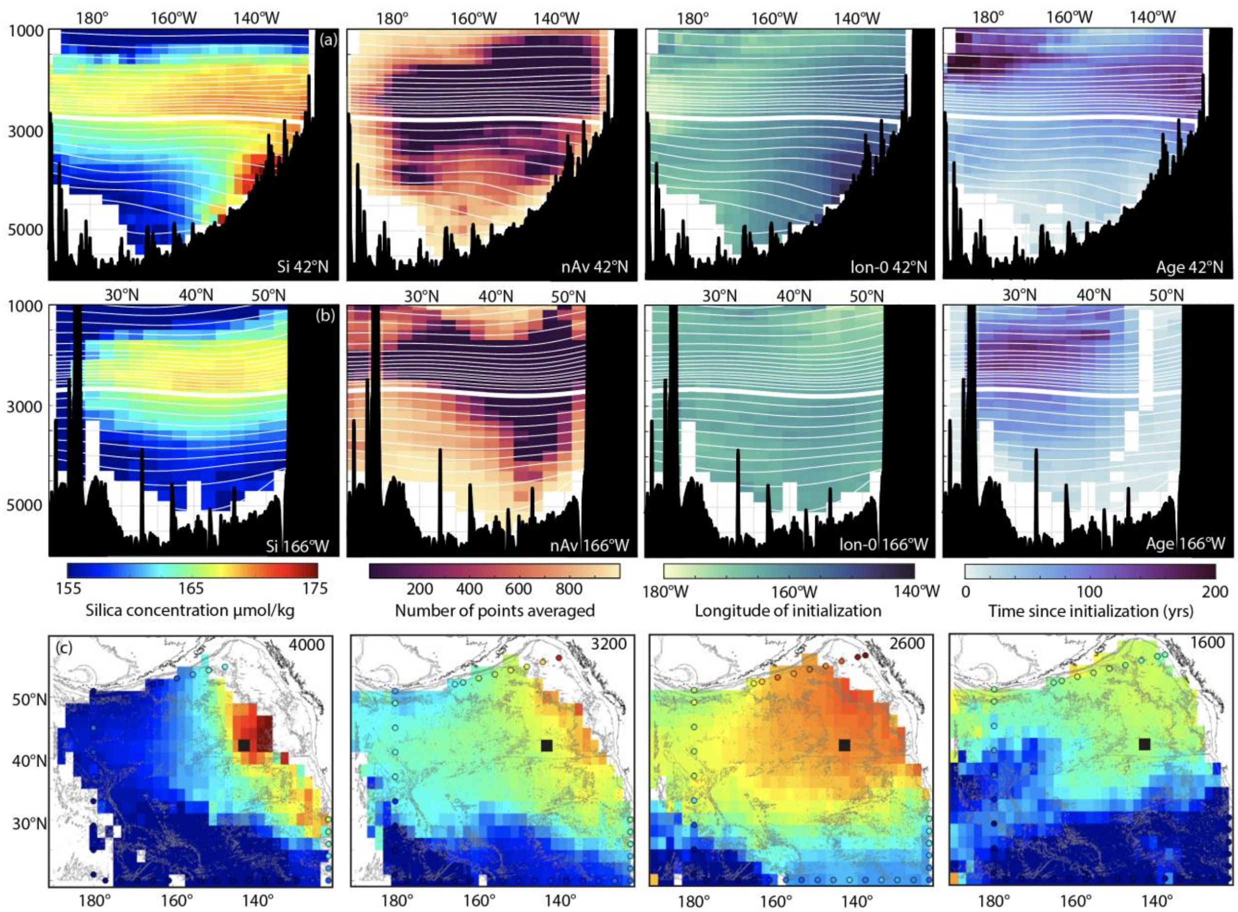

Figure 1. Vertical sections along (a) 42°N and (b) 166°W, from left to right: Eulerian bin-average silica concentration, number averaged, average longitude of water parcel initialization, and time since initialization, with bathymetry from 0.5′ SRTM30-PLUS (Becker et al., 2009; Sandwell and Smith, 2009). White lines indicate neutral surfaces. The thicker white line is γ = 28.016, the uppermost neutral surface within the UCDW. (c) Modeled silica concentration on constant pressure planes as indicated (dbar). The black square marks 42°N, 142°W. The colored circles indicate initial value concentration.

In Hautala (2018), lateral diffusivity, K_H, was modeled as independent of geographical location but a function of neutral density. It is not statistically significant within error bars reaching about ±200 m^2/s at mid-depth. Although weak, the exact value significantly impacts residence time in the tracer model. We use the "clock" associated with radiocarbon to determine an appropriate value for lateral diffusivity that does not excessively exceed the inverse model's of uncertainty (Supplement, Section D). We iteratively increase K_H, re-running the inverse calculation with specified (constant) diffusivity to determine an internally consistent flow field for the Lagrangian integrations. Lower values of K_H result in a basin-averaged low bias in radiocarbon, compared to observational values determined by linearly interpolating the model fields to bottle locations from four repeat sections (Figure 2, S-C1) that cross the NEPB (*P17*: Musgrave et al. 1995; *P16-2006*: Feely et al. 2013; *P01-2007*: Kawano et al. 2009 and *P02-*

2012: Swift et al. 2014). As K_H increases, radiocarbon bias improves, but silica bias worsens, as does the misfit to potential vorticity and salinity conservation equations in the inverse model. We settled on a displacement standard deviation of 90 km, corresponding to K_H = 260 m^2/s. This value of lateral mixing is less than half that of the "LOW-ISO" run from DeVries and Holzer (2019). However, tracer release experiments in abyssal Brazil Basin are consistent with even lower values (Rye et al. 2012). Likely, abyssal lateral diffusivity varies geographically in ways that are not currently well understood.

Next, we determine conditions for halting integration of Lagrangian trajectories. If a water parcel leaves the inverse model domain across 170°E or 20°N, integration is halted. Water parcels encountering interior topographic obstacles (i.e., missing value holes in the inverse domain) are assumed to enter a narrow, unresolved boundary current, such that flow is around the obstacle rather than dead-ending. In these cases, a "boundary current slippage" algorithm is implemented as follows. First, we divide the basin into eastern and western regions. The western region is between 173°W and 150°W, and north of the Hawaiian Ridge, defined as a line from (20°N, 150°W) to (32°N, 170°E). Here, if a topographic hole is encountered, the velocity is set purely eastward (i.e., back toward the interior) for one time step at the same speed prior to encountering the obstacle. The eastern region is between 150°W and 123°W and north of 20°N. Here, the velocity is set to purely westward (again, back toward the interior). Tracer concentration is not changed during boundary current slippage, and integration is halted if more than 20 sequential "slippage" time-steps occur (some water parcels repeatedly re-enter topographically masked regions and become stuck). In the eastern region, this process can be activated where neutral surfaces intersect the broad topographic slope. However, the density structure in these areas is such that geostrophic flow is predominantly along rather than across topographic contours. Thus, when the smaller across-topography component of flow results in trajectories leaving the domain, intermittent redirection into the nearest interior box has only a minor impact on the trajectories. Very few water parcels remain stuck in the interior after the maximum integration time of 500 years (Figure 3a, solid vs. dashed lines). The double silica maximum occurs without boundary slippage (Fig. S-D4), but with fewer points to average overall, particularly in the UCDW.

2.3 Tracer source/sink functions

Finally, we use existing observations to specify tracer source/sink functions that determine iterative concentration changes along the Lagrangian trajectories. We fit the Martin function (Martin et al., 1987) to deep sediment traps deployed from 200 to 4200 m depth at station P (50°N, 145°W; Wong et al. 2008) to obtain an estimate of the organic and inorganic carbon rain rate north of 40°N and its depth dependence. The resulting *b* value for organic carbon of 0.575 is close to that recommended by Marsay et al. (2015). The decrease in particulate flux as material settles through each layer should equal the remineralization rate, so the Martin function for each phase has been used to determine the losses of both organic C and $CaCO_3$ particulates. Fluxes have been defined for various latitude bands, with carbon fluxes for 20-35°N and 35-40°N taken as 25% and 50% of those for >40°N, respectively. For ^{14}C, pre-bomb estimates for $^{14}C/^{12}C$ in surface water have been used for remineralized particles, as bomb contamination has only been present for a small fraction of the 1-2 kyr residence time of the water below 1 km. Surface water $^{14}C/^{12}C$ ratios relative to atmospheric have been assumed as 0.95, 0,93 and 0.90 for the three latitude bands considered. For Si, there is an even stronger change in flux with latitude, as shown by benthic flux estimates from pore water profiles and core incubations, as well as in deep trap deployments (Hou et al., 2019). Sediment trap measurements at 1 and 4 km depth (Wong et al., 1999) indicate that the fraction of the rain at 1 km that dissolves while settling through the water column is undetectable, previously estimated at about 5% by Hammond et al. (2004). Regeneration is larger in the subarctic gyre, but the results are not sensitive to this increase (see Supplement, section D), nor to changes in silica source parameters by factors of two. Only a few percent of the particulate fluxes are buried (Hou et al., 2019), so the particle flux that does not dissolve while settling is assumed to be introduced into the deepest neutral density layer as the bottom source.

Zone	Si_B (mmol/m^2/year)	Si_R (mmol/m^2/year)	F_R	F_{C14}
5°N to 35°N	20	1	0.25	0.95
35°N to 40°N	200	10	0.5	0.93
> 40°N	600	90	1.0	0.90

Table 1. Parameters for the silica, carbon and radiocarbon source functions.

With these constraints in mind, we specify both a per volume water column regeneration source, Si_R, and a bottom source, Si_B. The latter affects only the deepest neutral surface, with a strength that depends on the height of this neutral surface above the bottom (h). Thus, the rate of change is, in µmol kg^{-1} yr^{-1},

$$\frac{\Delta \mathrm{Si}}{\Delta t} = \frac{1000}{\rho_0}\left(\frac{\mathrm{Si}_R}{H} + \frac{\mathrm{Si}_B}{h}\right)$$

where the latitude-dependent values are given in Table 1, the nominal ocean depth H = 5000 m, ρ_0 = 1025 kg/m^3, and the factor of 1000 has units of µmol/mmol.

Total C and ^{14}C changes (µmol kg^{-1} yr^{-1}) are handled similarly:

$$\frac{\Delta \mathrm{C}}{\Delta t} = \frac{1000}{\rho_0}(\mathrm{C}_R + C_B).$$

However, unlike silica, the "rain" component for C is a function of scaled pressure $\hat{p} = p/200$ dbar. The Martin function fits define constants, so that (in $m$mol m^{-3} y^{-1}),

$$\mathrm{C}_R = F_R(1.590\hat{p}^{-1.575} + 0.354\hat{p}^{-1.235})$$

$$\mathrm{C}_B = 1000\frac{F_R}{h}(0.553\hat{p}^{-0.575} + 0.301\hat{p}^{-0.235}).$$

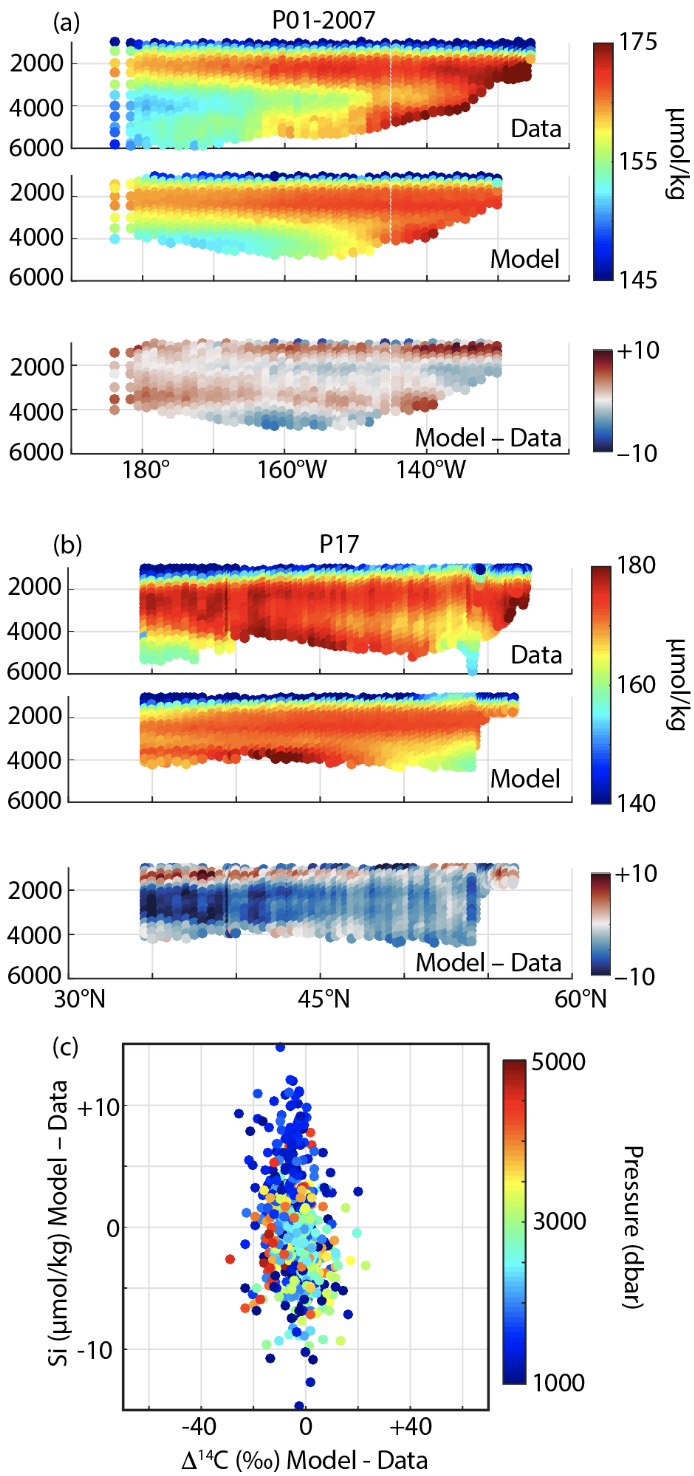

183

184 **Figure 2**. Vertical sections of modeled and observed Si along (a) P01-2007 and (b) P17. Note
185 that the model does not extend as deeply as the data, which reaches into low silica LCDW in
186 disconnected deep pools of the northern and southern NEPB. (c) Differences (model minus
187 observed) for ^{14}C vs Si using data from all four comparison sections.

Example values (mmol m^{-3} y^{-1}) for the northern zone (F_R =1) at 1000 dbar are C_R = 0.0175; at 4000 dbar: C_R = 0.023, and $C_B \times h/1000$ = 0.248 mol m^{-2} yr^{-1}.

The radiocarbon source function assumes a latitude-dependent fraction, F_{C14}, of the atmospheric value (Table 1), and a decay constant $\lambda = 1.209 \times 10^{-4}$ y^{-1}:

$$\frac{\Delta^{14}\mathrm{C}}{\Delta t} = F_{C14}\frac{\Delta \mathrm{C}}{\Delta t} - \lambda^{14}\mathrm{C}.$$

3 Results

Eulerian tracer fields are created by averaging points from all ensembles in 2° x 2° x 200 dbar bins (Figure 1 and Supplement, section B). Trajectories do not sample the deepest parts of the basin (white areas of Figure 1), particularly in the west, where isolated pools of LCDW and dense UCDW exist. Outside these unresolved areas, the model predicts the overall tracer structure well, particularly the existence of the double silica maximum in the eastern NEPB (Figure 2). The average absolute difference from observations between 1500-3500 dbar is about 1% for silica and radiocarbon and less for total carbon (Figure S-D1). Between 1500 and 3500 dbar, the standard deviation of tracer difference from observations is: radiocarbon – 6.9‰, silica – 6.1 µmol/kg and total carbon – 11.5 µmol/kg. This degree of misfit for radiocarbon is similar to that of DeVries and Holzer (2019).

Figure 3a shows how basin-averaged silica concentration changes as a function of time, averaged over all trajectories, and separately for the NPDW and UCDW. Also shown is the distribution of years spent within the basin, excluding water parcels that leave the basin within the first 25 years (across boundaries close to their release location). The inferred bulk advective transit time is roughly 40-100 years, larger in the NPDW than the UCDW. Concentration changes more rapidly near the beginning of integration reflecting time spent beneath the subarctic gyre with its higher silica flux, particularly for the UCDW. However, there is considerable geographic variation in silica addition to the UCDW (Figures 3c, S-B2), due to the bottom source contributing elevated silica primarily where neutral surfaces ground into topography. Here, rates of silica addition reach 2 µmol kg^{-1} yr^{-1} at 4000 dbar (Figure S-B3) within associated with the southward near-bottom current in the eastern half of the basin.

4 Discussion and conclusions

A double silica maximum is not found in the boundary conditions (Figures 1c, S-A1). The northern initialization line has a silica maximum in the lower NPDW (γ = 28.0) that increases eastward from 166 µmol/kg at (51°N, 180°) to 177.3 µmol/g at (56.7°N, 137°W). Values at γ = 28.1 (the top of the *Lower* Circumpolar Deep Water, LCDW) also increase towards the east, by more than double the amount at the maximum (153.2 to 176.1 µmol/kg). The Aleutian Trench must act as a source of silica to bottom water flowing east (and possibly recirculating) in the Aleutian deep boundary current system, establishing a zonal gradient in silica concentration that contributes to the eastward intensification of both silica maxima in the interior. As discussed in what follows, the double silica maximum itself arises from the geometry of lateral advective pathways combined with the bottom source.

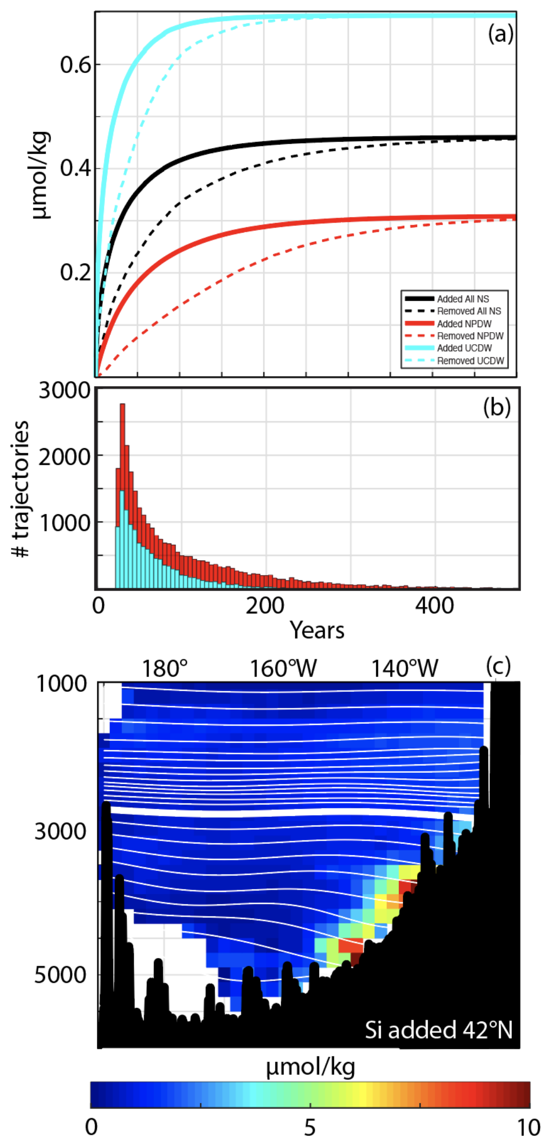

Figure 3. (a) Along-trajectory silica concentration as a function of years since initialization for all water parcels (black), NPDW (red) and UCDW (blue). Solid lines show the average value at a given year over all water parcels remaining within the basin. Dashed lines show the average value for water parcels exiting at that time. (b) Distribution of time between release and exit for NPDW (blue) and UCDW (red). A large number of trajectories exit within 25 years across nearby boundaries and are excluded from this histogram. (c) Silica added (Eulerian bin-averaged) along 42°N, defined as concentration of a water parcel minus its initial value.

In the NPDW, silica values in the pre-existing mid-depth maximum are augmented modestly and uniformly within the basin (Figures 3c, S-B2). Weak diapycnal mixing implies very little vertical transport from the UCDW to the NDPW. The total Eulerian diapycnal transport across the separating γ=28.01 surface is only 0.1 Sv, about 3% of the 3.5 Sv abyssal inflow from the northern boundary below 3000 m (Hautala 2018). From the Lagrangian perspective, only 0.6% of the water mass trajectories cross to lighter water across γ=28.01, and none of these were initialized on surfaces denser than γ=28.016, corresponding to the lightest neutral surface within the UCDW.

Talley and Joyce (1992) calculated about 0.2 µmol L^{-1} yr^{-1} to maintain the mid-depth (NPDW) silica maximum. Their budget assumed a 20 µmol/kg average North Pacific enhancement of silica over its value in the western tropics (140 µmol L^{-1}), and a time-scale of 100 years based on the western vs. eastern difference in ^{14}C at its minimum. Johnson et al. (2006) used a similar approach for a regional NEPB estimate, relative to a 160 µmol L^{-1} value near Hawaii. An updated inventory calculation resulted in an excess silica pool of approximately 164 Tmol between 2000-3000 dbar. Nominal westward flow of 0.5 cm/s resulted in a flux of 2.4 Tmol/yr, larger than obtained (1.6 Tmol/yr) using the radiocarbon residence time of Talley and Joyce (1992).

We can compare these earlier estimates to the average accumulated silica concentration, converting to total silica using the combined mass of the Eulerian bins. For the NPDW as a whole (approximated using bins between 1000-2800 dbar), 29 Tmol is added. The average time since initialization, or age, is 86 years, and the average supply rate is 0.3 Tmol/yr, calculated by averaging bin values of added silica divided by age. Silica is added primarily by water column regeneration, and this rate is 5 to 10 times smaller than the earlier estimates, and supporting the idea that the NPDW maximum is largely advecting through the basin with relatively minor modification. The inverse model suggests that a more appropriate scale value for advective velocity in the NPDW is 0.1 cm/s (Hautala 2018), explaining part of the difference from Johnson et al. (2006). In addition, the lower NPDW primarily enters the basin from the north, raising the concentration of "background" silica water by 6 to 17 µmol/kg (based on the zonal range of initial Si along the northern initialization line).

The model tends to underpredict Si below 2000 dbar (Figure 2c), an overall bias that cannot be corrected by tuning parameters without exacerbating the low radiocarbon bias (Supplement, section D). Along P17 (Figure 2b), the NPDW silica deficit is especially large south of ~48°N, proximal to gaps in the Juan de Fuca Ridge where higher silica Cascadia Basin Bottom Water overflows (Hautala et al. 2009). Talley and Joyce (1992) hypothesized that Cascadia Basin was a source for mid-depth Si, however benthic flux measurements show that it can contribute only ~0.06 Tmol/y (Esther et al. 2010), about 20% of the overall NPDW input in our tracer model. Although not properly resolved on the large scale of the inverse circulation fields, a sensitivity experiment with a crude representation of silica flux from Cascadia Basin suggests that it may be partially responsible for the regional low values in the tracer model at mid-depth along P17 (Figure S-D2).

In contrast to the situation at mid-depth, silica concentration within the UCDW layer is strongly modified within the NEPB. North of 30°N, this water mass is primarily sourced from the northern boundary, flowing to the south along topography east of 150°W, associated geostrophically with neutral surfaces that slope downward to the east (Hautala 2018, Figures 1a, S-D3). Water parcels preferentially acquire silica from the bottom source in regions where these neutral surfaces ground, or incrop, into the seafloor that slopes upward to the east. The incrop longitude shifts further east for lighter surfaces, resulting in lower silica water above higher silica water in the UCDW layer at any given location (Figure 1a, c). A weak near-bottom maximum in total carbon is also created, in agreement with the data along P01-2007 (for carbon fields, see the Supplement). At 4000 dbar, Si is elevated by 5-10 µmol/kg over the initial value in an area east of 150°W (Figure 1c), before becoming admixed with lower Si water to the south. In total, the UCDW (2800-5000 m) gains 35 Tmol, primarily from the seafloor source. The average age is 40 years, and the average supply rate is 1.4 Tmol/year, primarily in the eastern subarctic gyre. A spatial correlation between young age and high silica flux makes the average supply rate substantially larger than the total silica added divided by the average age.

We conclude:

(1) The mid-depth silica maximum in the lower NPDW is largely flowing through the basin with minimal modification, consistent with the original hypothesis of Edmond et al. (1979). The increase in silica at the maximum towards the east along the northern tracer initialization line suggests the importance of processes associated with the Aleutian deep boundary current system, but these are unresolved by the present study.

(2) The near-bottom maximum in the UCDW is created locally within the basin, consistent with the independent analysis of Hou et al. (2019) based on benthic flux measurements and one-dimensional modeling of the bottom 500 m of the water column. The addition of silica via the seafloor source occurs preferentially where neutral surfaces incrop into broadly upsloping topography.

The observed silica structure is fundamentally dependent on vertically disconnected circulation systems in the UCDW and the NPDW, supported by weak diapycnal mixing in the inverse solution of Hautala (2018). We note that diapycnal mixing in Hautala et al. (2018) is considerably weaker than in the adjoint inverse model of DeVries and Holzer (2019), and full verification awaits direct measurement. However, weak diapycnal mixing in the interior NEPB is supported by the observations that do exist (Kunze 2017). The inverse calculation is limited to large scales, and unresolved mixing hotspots may provide localized places where water parcels, with high concentrations in the UCDW may move into NPDW density classes (Hautala 2018). Indeed, observed high silica concentrations connect the deep and mid-depth maxima in a very limited band just north of 40°N along P17 (Figure 2b). The Mendocino Fracture Zone may be one mixing hotspot – it has a crest that reaches well into the NPDW, and is known to have elevated diapycnal mixing rates in its immediate vicinity (Althaus et al. 2003).

Finally, given diapycnal mixing rates that decrease away from the seafloor, there is very little diapycnal communication within the NPDW itself and its treatment as a single water mass is likely an oversimplification. Water parcels may exit the basin and recirculate west of the Hawaiian Ridge to re-enter the system at somewhat lighter density. Circuits that include the southern hemisphere cannot be ruled out, suggesting a future extension of the model to the entire Pacific. The noncoincidence of diverse tracer extrema such as silica, oxygen, nutrients, carbon, radiocarbon and ^{3}He (e.g Fig. S-B1, S-B2, Lupton 1998; Talley et al. 1991) in the northeast Pacific are difficult to explain. We hypothesize a new schematic involving a slow upward spiral of deep water parcels making multiple long circuits that pass through the Northeast Pacific Basin on successively lighter density horizons. This many-layered circulation system, combined with the unique source/sink aspects of each tracer feeding into different portions of the upward spiralling trajectories, may have better success in explaining the observed complexity in the tracer features in this region.

Acknowledgments and Data

The data underlying this study are in the public domain or otherwise published as noted in the text. The absolute geostrophic flow and neutral surface property fields (Hautala 2018), currently available on Hautala's faculty website at http://faculty.washington.edu/hautala/Atlas, and the final version of the electronic Supplement will be submitted for permanent archive with UW ResearchWorks upon acceptance of the manuscript.

References

Althaus, A. M., E. Kunze and T. B. Sanford (2003). Internal tide radiation from Mendocino Escarpment. J. Phys. Ocean. 33: 1510-1527.

DeVries, T. and M. Holzer (2019). Radiocarbon and helium isotope constraints on deep ocean ventilation and mantle-3He sources. J. Geophys. Res.: 2018JC014716.

Edmond, J. M., S. S. Jacobs, A. L. Gordon, A. W. Mantyla and R. F. Weiss (1979). Water column anomalies in dissolved silica over opaline pelagic sediments and the origin of the deep silica maximum. J. Geophys. Res. 84 (C12): 7809-7926.

Esther, T. A., D. E. Hammond, S. L. Hautala, H. P. Johnson, R. J. Schwartz and A. N. Paukert (2010). Evaluation of the budget for silicic acid in Cascadia Basin deep water. *Deep-Sea Research I* 57: 677-686.

Feely, Richard A.; Sabine, Christopher L.; Millero, Frank J.; Langdon, Chris; Fine, Rana A.; Bullister, John L.; Hansell, Dennis A.; Carlson, Craig A.; McNichol, Ann; Key, Robert M.; Byrne, Robert H.; Wanninkhof, Rik (2013). Partial pressure (or fugacity) of carbon dioxide, dissolved inorganic carbon, pH, alkalinity, temperature, salinity and other variables collected from discrete sample and profile observations using Alkalinity titrator, CTD and other instruments from THOMAS G. THOMPSON in the Gulf of Alaska, North Pacific Ocean and South Pacific Ocean from 2006-02-13 to 2006-03-30 (NODC Accession 0108062). Version 2.2. National Oceanographic Data Center, NOAA.

Hammond, D. E., J. McManus and W. M. Berelson (2004). Oceanic germanium/silicon ratios: Evaluation of the potential overprint of temperature on weathering signals. *Paleoceanography* 19: doi:10.1029/2003P A000940

Hautala, S. L., H. P. Johnson and D. E. Hammond (2009). Bottom water circulation in Cascadia Basin. Deep-Sea Res. I 56, 1688–1707.

Hautala, S. L (2018). The abyssal and deep circulation of the Northeast Pacific Basin. Prog. Oceanogr. 160: 68-82.

Hou, Y., D. E. Hammond, W. M. Berelson, N. Kemnitz, J. F. Adkins and A. Lunstrum (2019). Spatial patterns of benthic silica flux in the North Pacific reflect upper ocean production. *Deep-Sea Res. I* 148: 25-33.

Johnson, H. P., S. L. Hautala, T. A. Bjorklund and M. R. Zarnetske (2006). Quantifying the North Pacific silica plume. *Geochemistry, Geophysics and Geosystems* 7: doi:10.1029/2005GC001065.

Kawano, T., H. Uchida and T Doi (2009). WHP P01, P14 Revisit Data Book: Field Activity of JAMSTEC towards International Repeat Hydrography and Carbon Program, 2007. Japan Agency for Marine-Earth Science and Technology.

Kunze, E., Firing, E., Hummon, J.M., Chereskin, T.K., Thurnherr, A.M., (2006). Global abyssal mixing inferred from lowered ADCP shear and CTD strain profiles. *J. Phys. Oceanogr*. 36, 1553–1576.

Kunze, E. (2017). Internal-wave-driven mixing: global geography and budgets. J. Phys. Ocean. 47: 1325-1345.

Macdonald, A.M., Mecking, S., Robbins, P.E., Toole, J.M., Johnson, G.C., Talley, L., Cook, M., Wijffels, S.E., 2009. The WOCE-era 3-D Pacific Ocean circulation and heat budget. Prog. Oceanogr. 82, 281–325.

Marsay, C.M., R.J. Sanders, S.A. Henson, K. Pabortsava, E.P. Achterberg, and R.S. Lampitt (2015) Attenuation of sinking particulate organic carbon flux through the mesopelagic ocean. *Proc. Nat. Acad Sci.* 112 (4): 1089-1094.

Martin, J. H., G. Knauer, D. Karl, D. and W. Broenkow (1987). VERTEX: Carbon cycling in the northeast Pacific, *Deep-Sea Res*. *I* 34: 267–285.

Musgrave, D., M. Aoyama, R. M. Key and P. D. Quay (1995). Final Cruise Report: World Ocean Circulation Experiment Pacific Ocean P17N. CLIVAR and Carbon Hydrgraphic Data Office. https://cchdo.ucsd.edu/cruise/325021_1.

Rye et al. (2012). Diapycnal diffusivities from a tracer release experiment in the deep sea, integrated over 13 years. Geophys. Res. Lett. 39: 2011GL050294.

Schmitz Jr, W.J., 1995. On the interbasin-scale thermohaline circulation. Rev. Geophys. 33, 151–173.

Swift, James H.; Mecking, Sabine; Feely, Richard A.; Dickson, Andrew G.; Carlson, Craig A.; Jenkins, William J.; McNichol, Ann; Key, Robert M.; Ho, David T.; Sigman, Daniel; Macdonald, Alison M.; Buesseler, Ken; Martz, Todd R. (2014). Dissolved inorganic carbon, pH, alkalinity, temperature, salinity and other variables collected from discrete sample and profile observations using CTD, bottle and other instruments from MELVILLE in the North Pacific Ocean and Philippine Sea from 2013-03-21 to 2013-05-01 (NODC Accession 0117338). Version 3.3. National Oceanographic Data Center, NOAA. Dataset. doi:10.3334/CDIAC/OTG.GOSHIP_P02_318M20130321

Talley, L. D., T. M. Joyce and R. A. de Szoeke (1991). Transpacific sections at 47°N and 152°W: distribution of properties. Deep-Sea Res., 38 (S1): S63-S82.

Talley, L. D. and T. M. Joyce (1992). The double silica maximum in the North Pacific. J. Geophys. Res. 97 (C4): 5465-5480.

Taylor, G. I. (1921). Diffusion by continuous movements. Proc. London Math. Soc., 20, 196-212.

Warren, B. A. and W. B. Owens (1985). Some preliminary results concerning deep northern-boundary currents in the North Pacific. Prog. Oceanogr. 14, 537–551.

Wong, C.S., F.A. Whitney, D.W. Crawford, K. Iseki, R.J. Matear, W.K. Johnson, J.S. Page, and D. Timothy (1999). Seasonal and interannual variability in particle fluxes of carbon, nitrogen and silicon from time series of sediment traps at Ocean Station P, 1982-1993: relationship to changes in subarctic primary productivity, Deep-Sea Res. II 46, 2735-2760, 1999.